JOURNAL OF COMPUTATIONAL PHYSICS 22, 229–244 (1976)

Finite Element Models for Creeping Convection

ATUO SATO

Graduate Research Assistant

AND

ERIK G. THOMPSON

Professor of Civil Engineering, Colorado State University, Fort Collins, Colorado 80523

Received October 9, 1975; revised March 9, 1976

Finite-element thermal-mechanical models for creeping convection are developed. Examples using both quasi-Lagrangian and Eulerian formulations are presented and compared. Steady-state and transient problems are treated with attention paid to stress free boundaries.

1. INTRODUCTION

The equations governing the incompressible creeping flow of a viscous fluid are often coupled with the equation for heat transfer to describe a number of physically significant phenomena. Among these are plastic flow during metal forming processes, velocity fields associated with the lubrication of bearings, and convection within the earth's mantle. The coupling may be weak to fairly strong depending on the particular application.

The most common types of coupling are those due to temperature dependent viscosity, heat sources due to viscous dissipation, and heat transfer due to convection. An additional coupling also occurs in free convection due to variations in density resulting from thermal gradients. This latter phenomenon is believed to occur within the earth's mantle and presently affords the most plausible explanation for the moving crustal plates. It is this specific problem which is addressed in this paper.

Since the advent of the new global tectonics there has been a number of papers devoted to finite amplitude creeping convection. Early work in this area focused on analytical methods as well as combined analytical and numerical techniques.

Turcotte and Oxburgh [11] review this literature which includes perturbation methods, Fourier analysis, boundary layer approaches, and finite-difference techniques.

Much of the recent literature has concentrated on the finite-difference method. Steady-state solutions have been obtained by iterative techniques (Torrance and Turcotte, [10]) as well as incremental integration in time (e.g., Andrews, [1]). When proper initial conditions are known, the latter approach provides a history of the convection.

This paper reports on a new approach to the solution of these equations by the finite-element method. Of particular significance are (a) the use of either an Eulerian or a quasi-Lagrangian frame of reference, (b) the ability to easily treat free surfaces, and (c) a fast convergence to steady-state conditions.

2. Governing Equations and Finite Element Formulation

Creeping Viscous Flow

The equations governing the creeping flow of an incompressible viscous fluid are

$$\sigma_{ij,j} + \rho X_i = 0 \tag{1}$$

$$u_{i,i} = 0 \tag{2}$$

$$\sigma_{ij} = -p\delta_{ij} + 2\mu\epsilon_{ij} \tag{3}$$

$$\epsilon_{ij} = \tfrac{1}{2}(u_{i,j} + u_{j,i}) \tag{4}$$

$$\sigma_{ij}\nu_j = \overline{T}_i \quad \text{on} \quad S_\sigma \tag{5}$$

$$u_i = \bar{u}_i \quad \text{on} \quad S_u \tag{6}$$

where σ_{ij} is the stress tensor, ρ is the density, X_i is the body force per unit mass, u_i is the velocity, p is the pressure, μ is the viscosity, ν_j is the unit normal vector to the surface. $\overline{T}_i$ is the specified surface traction on S_σ, and $\bar{u}_i$ is the specified velocity on the surface S_u.

Equations (1), (2), and (5) are the Euler equations for the functional

$$J = \int_V \tfrac{1}{2}\mu\epsilon_{ij}\epsilon_{ij}\,dV - \int_{S_\sigma} \overline{T}_i u_i\,dS - \int_V p\epsilon_{ii}\,dV - \int_V \rho X_i u_i\,dV \tag{7}$$

when extremized with respect to p and all u_i satisfying Eq. (6). The pressure term in Eq. (7) serves as a Lagrange multiplier for the constraint condition (2).

The usual finite-element formulation now can be made with approximate solutions to Eqs. (1)–(6) found through the condition

$$\delta J = 0. \tag{8}$$

This particular approach to the finite element analysis of incompressible creeping flows was first proposed by Thompson, Mack, and Lin [9] and later expanded by Thompson and Haque [8]. Similar approaches have been used for incompressible elastic solids (Herrmann, [3]; Oden, [6]; Hughes and Allik, [4]). The variation (8) when taken with respect to p requires

$$\delta J = -\int_V \delta p \, \epsilon_{ii} \, dV = 0 \tag{9}$$

for arbitrary δp. If Eq. (2) is to be satisfied as a consequence of Eq. (9), the approximation chosen for p must be complete with respect to the approximation for ϵ_{ii}. When this is the case, there will exist a δp proportional to ϵ_{ii} such that

$$\delta p = C\epsilon_{ii} \tag{10}$$

which allows Eq. (9) to be written as

$$\delta J = -C\int_V \epsilon_{ii}\epsilon_{jj} \, dV = 0. \tag{11}$$

This equation is only satisfied if Eq. (2) is met everywhere in V. If, therefore, a polynomial of degree N is used to approximate u_i within an element volume V_e, a polynomial approximation of degree $N - 1$ should be used for the pressure p. The resulting finite-element approximation is referred to as complete incompressibility (Thompson and Haque, [8]).

It is, however, not necessary to satisfy Eq. (2) everywhere to obtain convergence of the finite element method; in fact, faster convergence has been observed when this constraint is relaxed (Thompson, [7]). If within each element the pressure is taken as constant Eq. (9) can be written as

$$\delta p \int_{V_e} \epsilon_{ii} \, dV = 0 \tag{12}$$

which only requires

$$\int_{V_e} \epsilon_{ii} \, dV = 0 \tag{13}$$

for arbitrary δp. Equation (13) expresses an average incompressibility condition for each element. This later formulation is referred to as average incompressibility and was used for the examples presented in this paper.

Through the usual techniques associated with the finite element method (Thompson and Haque, [8]; Thompson, [7]; Zienkiewicz, [12]) we obtain by Eq. (8)

$$\begin{bmatrix} K & \vdots & G^T \\ \cdots & \vdots & \cdots \\ G & \vdots & 0 \end{bmatrix} \begin{Bmatrix} U \\ \cdots \\ -p \end{Bmatrix} = \begin{Bmatrix} F \\ \cdots \\ 0 \end{Bmatrix} \tag{14}$$

where $[K]$ is the usual stiffness matrix, $[G]$ is the constraint of incompressibility on the nodal point velocities $\{U\}$, $\{P\}$ is the matrix of nodal point pressures (Lagrange multipliers), and $\{F\}$ is the matrix of nodal point forces.

Heat Equation

The governing equations used to describe the time dependent temperature distribution in a convecting conducting fluid are

$$\rho c_p((\partial T/\partial t) + u_i(\partial T/\partial x_i)) = (\partial/\partial x_i)(k(\partial T/\partial x_i)) + Q \tag{15}$$

$$T = \bar{T} \quad \text{on} \quad S_T \tag{16}$$

$$(k(\partial T/\partial x_i) - \rho c_p u_i T)\, \nu_i = \bar{q} \quad \text{on} \quad S_q \tag{17}$$

$$\rho = \rho_0(1 - \alpha(T - T_0)) \tag{18}$$

where T is the temperature, k is the coefficient of thermal conductivity, Q is the heat source, $\bar{T}$ is the specified temperature on S_T, c_p is the specific heat at constant pressure, $\bar{q}$ is the specified heat flow across S_q, and α is the coefficient of thermal expansion. The source Q can result from viscous dissipation, radioactive heat generation, etc. depending on the specific problem of interest.

When the convective terms in Eq. (15) are removed, the resulting equation is for pure conduction and is applicable in the quasi-Lagrangian formulation described in Section 3 of this paper.

The inclusion of the convective terms in Eq. (15) rules out the possibility of using the Ritz formulation of the finite-element method, and we therefore turn to Galerkin's method. Because the general procedure is well domumented in the literature (Zienkiewicz, [12]) we provide here only an outline.

Let the finite-element approximation for temperature be given by

$$T = \sum_{\beta=1}^{n} N_{(\beta)} T_{(\beta)} \tag{19}$$

where $N_{(\beta)}$ and $T_{(\beta)}$ are the basis functions and temperatures associated with the n nodal points. The parentheses about the subscripts are used to avoid confusion with the indices used for Cartesian tensors.

The weighted residuals found for Eqs. (15) and (17) are

$$R_v = \sum_{\beta=1}^{n} \int_v \left\{ \left(N_{(\beta)} \frac{\partial T_{(\beta)}}{\partial t} + u_i \frac{\partial N_{(\beta)}}{\partial x_i} T_{(\beta)} \right) \rho c_p - \frac{\partial}{\partial x_i} \left(k \frac{\partial N_{(\beta)}}{\partial x_i} T_{(\beta)} \right) - Q \right\} N_{(\alpha)}\, dV \tag{20}$$

and

$$R_s = \sum_{\beta=1}^{n} \int_{S_q} \left\{ \left(k \frac{\partial N_{(\beta)}}{\partial x_i} T_{(\beta)} - \rho c_p u_i N_{(\beta)} T_{(\beta)} \right) \nu_i - \bar{q} \right\} N_{(\alpha)}\, dS. \tag{21}$$

We now seek values for either $\partial T_{(\beta)}/\partial t$ or $T_{(\beta)}$ which will cause the above residuals to vanish for all $N_{(\alpha)}$, α equal 1 through n. Integration by parts and the application of Green's theorem gives a set of n algebraic equations. We write them in matrix notation as

$$[H]\{T\} + [P]\{\dot{T}\} + \{Q\} = 0 \tag{22}$$

where $[H]$ results from both the gradient and convective terms in Eq. (20), $[P]$ derives from the coefficient of the time derivative of temperature in Eq. (20), and $\{Q\}$ contains the sources in V and on S expressed in Eqs. (20) and (21). The matrix $[H]$ is nonsymmetric due to the convective terms in Eq. (20).

If the time rates of change of the nodal point temperatures, $\{\dot{T}\}$, are known (e.g., identically zero for steady-state) Eq. (22) can be used to obtain the nodal point temperatures, $\{T\}$. For transient conditions when the nodal point temperatures are known at a given time, Eq. (22) yields the time derivatives of temperature. Although these derivatives can be solved for directly and used to numerically integrate the temperatures with time, it is more common to express the derivate in finite-difference form at times t and $t + \Delta t$ (Zienkiewicz, [12]). In this manner an implicit finite-difference scheme is used in time with a finite-element approximation of temperature in space. The resulting matrix equation is

$$[2[P] + [H]\,\Delta t]\{T\}_{t+\Delta t} = [2[P] - [H]\,\Delta t]\{T\}_t - 2\,\Delta t\{Q\}_{\text{ave}}\,. \tag{23}$$

where $[P]$ and $[H]$ are evaluated at time t, and

$$\{Q\}_{\text{ave}} = (1/\Delta t)\int_0^{\Delta t} \{Q\}\,dt. \tag{24}$$

or an appropriate approximation thereof.

3. Solution Techniques

The present finite-element formulation for the free convection of creeping fluids lends itself well to either a quasi-Lagrangian viewpoint or an Eulerian viewpoint. Both have particular advantages depending to a large extent on whether a steady-state solution is sought or a transient behavior is of interest.

The Quasi-Lagrangian Viewpoint

Due to the absence of the convective terms in the momentum equation, velocity can be solved for directly and, for Newtonian viscosity, is a function only of the instantaneous geometry and applied forces. It therefore is possible to interpret Eq. (14) as a quasi-Lagrangian formulation of the momentum equation and to allow

the mesh layout to flow with the fluid. This is easily accomplished by incrementing each nodal point coordinate by its corresponding velocity multiplied by the change in time for that increment. This procedure corresponds to simple Eulerian integration although more accurate methods are possible (Zienkiewicz, [12]). When the mesh layout flows with the fluid, the convective terms in the heat equation are no longer needed and, for this moving coordinate system, we have a case of pure conduction.

This approach has the obvious advantage of accommodating changes in geometry such as might occur at free surfaces and interfaces. When steady-state conditions are desired this method is not particularly desirable because of the distortion which can occur in the element layout with large amplitude flow and which eventually requires adjustment of the mesh.

The Eulerian Viewpoint

When Eq. (14) is taken as a pure Eulerian formulation, the mesh remains stationary in space and the convective terms must be included in the heat equation. If geometry changes are unimportant and steady-state conditions are desired, this approach is preferable. Its primary advantages are that the mesh layout does not become distorted with time and that steady-state convergence often can be obtained in three or four iterations for Rayleigh numbers two to three times the critical value. It was found that finer meshes and more iterations are needed with increasing Rayleigh numbers. Computations could be reduced, however, if a fine grid spacing were used in the boundary layers and a coarse spacing in regions of less importance.

The use of the time dependent heat equation to obtain steady-state conditions was found to be costly and is not recommended except for the case of free surface problems discussed below.

Free Surface Problems

An important feature of the finite-element formulation is that surface tractions can be specified directly. This need is most common in problems having free surfaces where the appropriate nodal point forces can be specified as zero on the right-hand side of Eq. (14).

For transient problems, the quasi-Lagrangian formulation allows one to follow free surface deformations with time. For such problems the finite element method is especially well suited. When steady-state free surface configurations are desirable, however, this approach may prove too expensive. In these cases, and when the surface topography is small, it is possible to arrive at a near steady-state condition using the Eulerian steady-state equations and the original surface topography. This usually can be obtained in a few iterations, after which the quasi-Lagrangian formulation can be used.

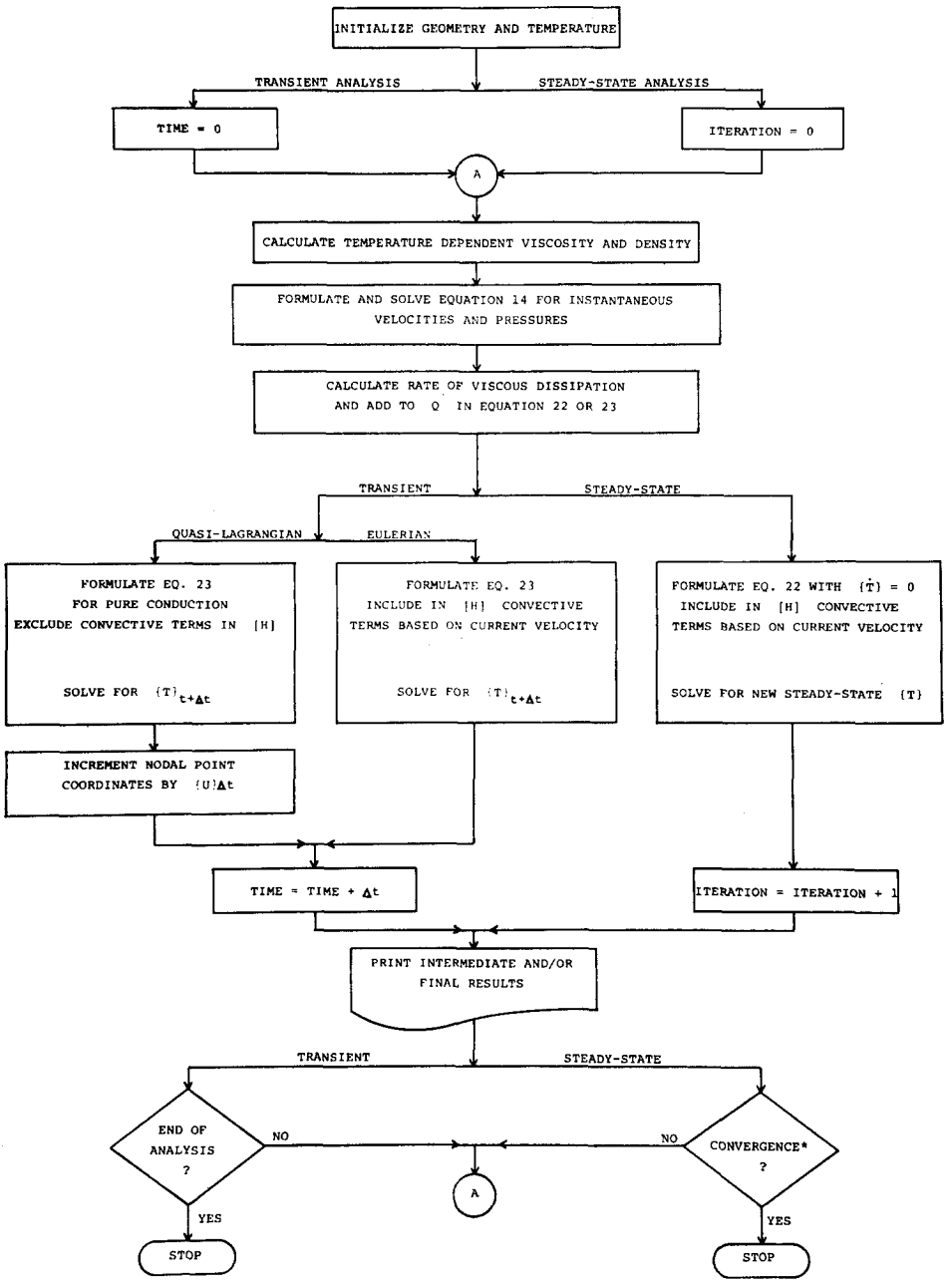

*Agreement with previous increment's steady-state velocity and temperature fields to within some specified accuracy

FIG. 1. Flow chart.

Solutions of Algebraic Equations

The matrix equations (14) and (23) are solved by Gauss elimination with a program written for sparse matrices. Care must be taken when solving Eq. (14) to avoid singularities during the elimination process. This occurs due to the constraint conditions for incompressibility appearing too soon in the elimination. These same constraint conditions also prevent iterative procedures, e.g., the Gauss–Seidel method, from converging.

The Basic Algorithms and Comparison of Methods

Several solution procedures have been described in the preceding material. Although these methods differ considerably in their individual advantages and disadvantages, they are remarkably similar in terms of their algorithms. The flow chart of Fig. 1 illustrates this similarity as well as the step-by-step procedure for each method. All methods can be conveniently incorporated into one computer code.

4. Illustrative Examples

Five examples are presented in this section. The first was chosen from the literature for comparative purposes. The next three illustrate quasi-Lagrangian and Eulerian formulations, effects of initial conditions on steady-state solutions, and the effect of mesh spacing on stability. The fifth example illustrates the technique used for arriving at steady-state free surface conditions.

All examples were solved using six-nodal-point isoparametric elements with average incompressibility. The numerical integration necessary for the formulation of the finite element matrices was carried out by a form of Gaussian quadrature (Zienkiewicz, [12]).

McKenzie, Roberts, and Weiss Model—Example 1

The finite-element approximation to creeping convection was first evaluated by comparing it with a finite-difference approximation reported by McKenzie, Roberts, and Weiss [5]. The specific problem consists of a square region of fluid in plane flow as shown in Fig. 2(a). The boundary conditions for velocity allow slip (zero shear stress) but there are no truly free surfaces, i.e., the fluid is completely contained within the square region shown. A horizontal temperature distribution, constant with time, is specified on the top surface, and the bottom surface is held at a constant uniform horizontal temperature. The two sides are insulated.

For the case of zero velocity, the steady-state temperature field is governed solely by conduction and is shown in Fig. 3(a). However, for any fluid of finite

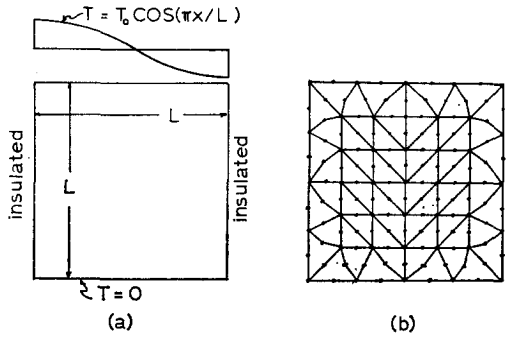

FIG. 2. Example 1. (a) Boundary conditions; (b) Mesh layout.

viscosity, a velocity field similar to that shown in Fig. 3(b) will result due to the horizontal variation in density and the vertical gravitational field. This clockwise convection drives the colder fluid on the right to the lower regions while forcing the warmer fluid on the left to rise. Steady-state is reached when the two modes of heat transfer, convection and condution, balance.

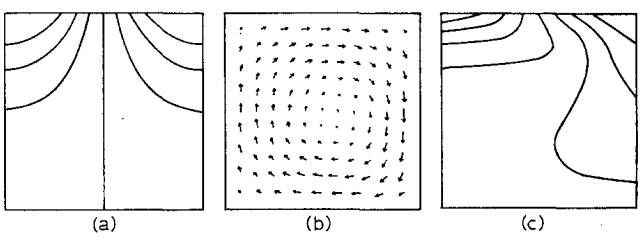

FIG. 3. Isotherms and velocity field for Example 1. (a) Steady-state conduction; (b) Typical velocity field; (c) Steady-state isotherms $R = 4580$.

Steady-state conditions were found by the procedure described in Fig. 1 for Rayleigh numbers equal to 45.8, 458.0, and 4,580.0 defined by McKenzie *et al.* as

$$R = g\alpha T_0 L^3/\kappa\nu. \tag{25}$$

The specific values for the variables in Eq. 25 are shown in Table I.

The initial temperature in each case was taken as the steady-state conduction field shown in Fig. 3(a). The maximum number of iterations to reach steady-state conditions (less than 0.1 % change in the maximum velocity between two successive iterations) was 5, and occurred for the largest Rayleigh number of 4580. The steady-state isotherms for this case are shown in Fig. 3(c). To within the accuracy of the plotted isotherms there were no discrepancies between the results found by the finite element model and those reported by MacKenzie *et al.* for the three Rayleigh numbers tested.

TABLE I

Material Parameters from McKenzie, Roberts, and Weiss [5]

$$\kappa = k/\rho\, c_p = 1.5 \times 10^{-6}\ \mathrm{m^2\ sec^{-1}}$$
$$\rho_0 = 3.7 \times 10^{3}\ \mathrm{kg\ m^{-3}}$$
$$c_p = 1.2 \times 10^{3}\ \mathrm{J\ kg^{-1}\ °C^{-1}}$$
$$g = 10\ \mathrm{m\ sec^{-2}}$$
$$\mu/\rho = 2 \times 10^{17}\ \mathrm{m^2\ sec^{-1}}$$
$$\alpha = 2 \times 10^{-5}\ \mathrm{°C^{-1}}$$
$$T_0 = 0.1,\ 1.0,\ 10.0$$

Quasi-Lagrangian and Eulerian Coordinates—Example 2

Both quasi-Lagrangian and Eulerian formulations were used to study the transient behavior of the previous problem for $R = 4580$. The initial condition was again the steady-state temperature for pure conduction. An incremant of time equal to 6.34 m year was used for the numerical integration. This time is equivalent to that needed for a particle to move approximately seven percent of the way through one of the double element squares of the original mesh if its velocity were equal to the maximum velocity found in the steady-state solution.

The results after 21 increments are shown in Fig. 4. The location along the element boundaries where the isotherms were found to cross are plotted in Fig. 4(a). The excellent agreement between the quasi-Lagrangian and Eulerian formulations is apparent.

The displaced mesh obtained from the quasi-Lagrangian model, Fig. 4(b), illustrates two interesting points. The first is that the middle region of the mesh has little distortion which indicates the nearly rigid rotation of this part of the cell. The second is the similarity between the zero isotherm and the displaced middle vertical line of the mesh, both shown in Fig. 4(c). Because this line was also the zero isotherm at time equal zero, their nearly perfect superposition in the lower region indicates the importance of convection at this high a Rayleigh number, as well as the fact that the steady-state condition shown in Fig. 3(c) has apparently not been reached.

Effect of Initial Conditions on the Steady-State Solution—Example 3

It was pointed out by Foster [2] that initial thermal conditions greatly affect the history and pattern of convection. This behavior was also found for steady-state solutions obtained by iteration of the Eulerian form of the steady-state equations. An example of this is shown in Fig. 5 where two steady-state solutions were found

for the same problem. The initial temperatures were deliberately chosen so as to create the desired two and three celle convection. For this same problem, however, attempts to obtain steady-state solutions having one cell and four cells failed, with the iteration procedure for both cases converging to a two cell configuration.

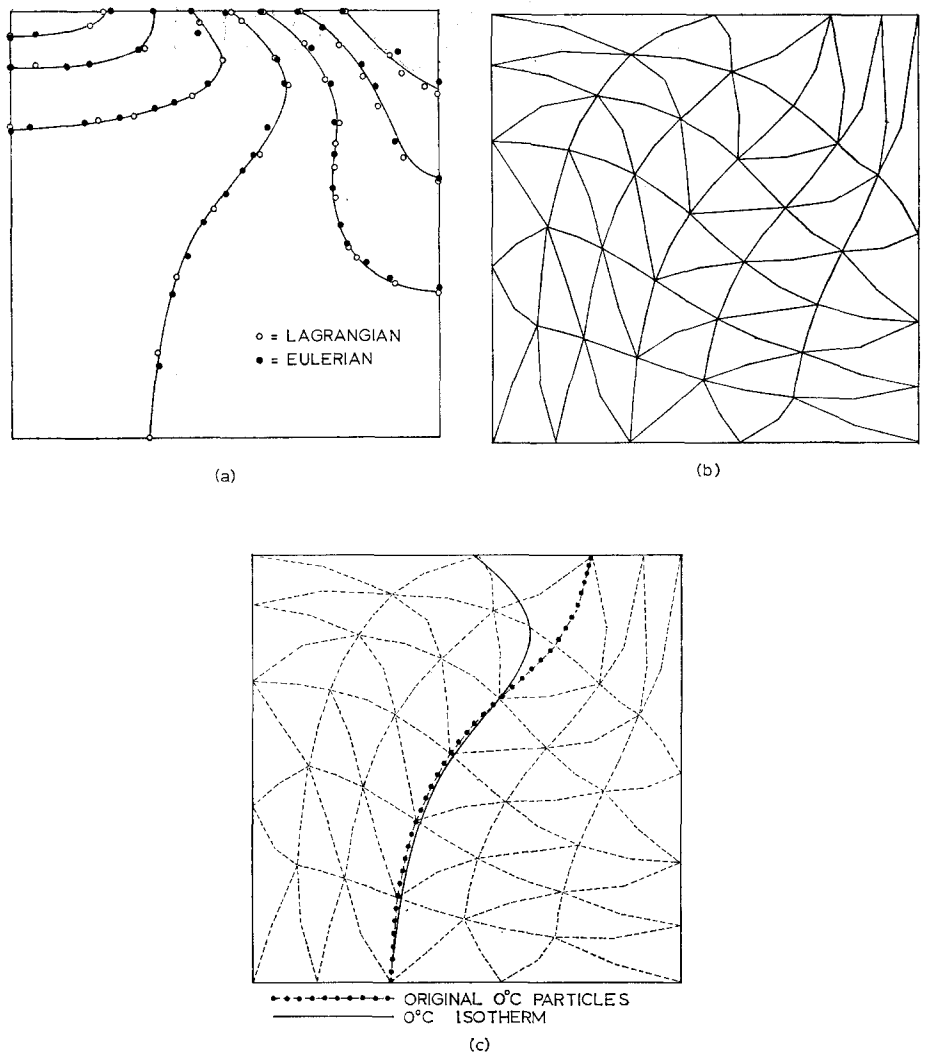

FIG. 4. Comparison of Lagrangian and Eulerian formulations for transient analysis, Example 2. (a) Temperature after 21 increments; (b) Lagrangian mesh after 21 increments.

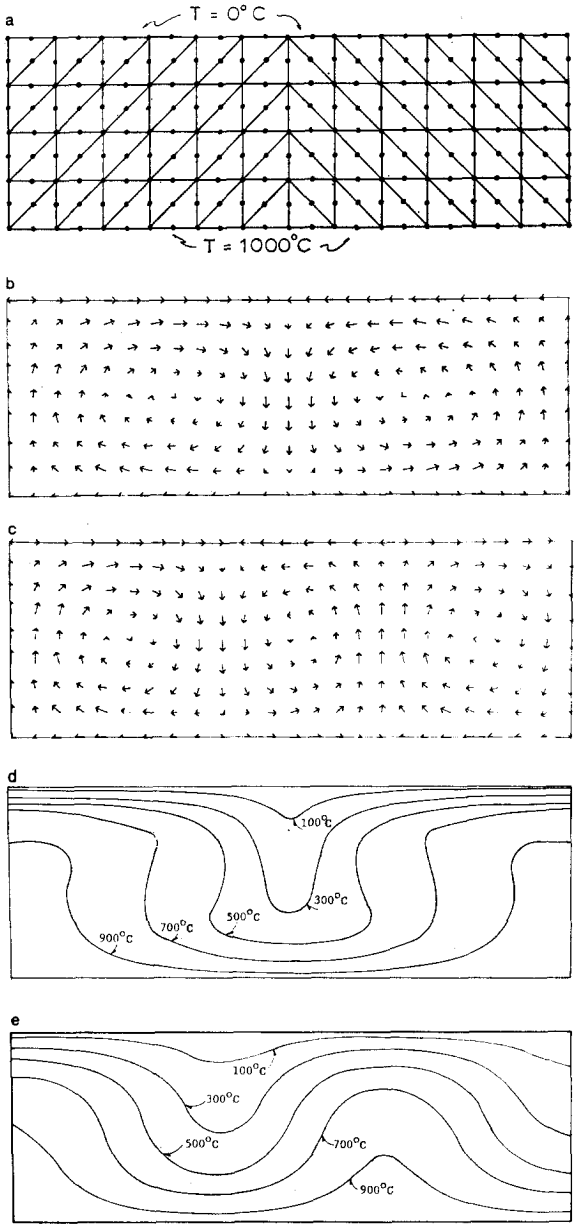

FIG. 5. Multiple steady-state solutions for $R = 1.739\,R_c$. (a) Mesh layout, (b) Steady-state two-cell convection, (c) Steady-state three-cell convection, (d) Isotherms for two-cell convection, (e) Isotherms for three-cell convection.

The parameters used in this example were the same as those used in the previous two examples with the exception of viscosity which was 2×10^{19} m^{2}sec^{-1}. The convection is driven by a uniform temperature on the lower boundary. The aspect ratio equals three and the Rayleigh number is 1143.5 or 1.739 times its critical value.

Effect of Mesh Spacing—Example 4

As the Rayleigh number is increased regions of high thermal gradients develop. When this occurs, the mesh spacing in these areas must be refined in order to maintain numerical stability. Although a thorough study of this problem has not been attempted, we present here an example of the difficulty.

Figure 5(a) shows the mesh used for the analyses of Rayleigh numbers equal to 1.739, 3.478, and 6.956 that of the critical value. However, at a value of 13.915 R_c, numerical instabilities resulted. After the mesh had been refined to that shown in Fig. 6(a), the iteration scheme converged to the stable steady-state patterns shown in Figs. 6(b) and 6(c).

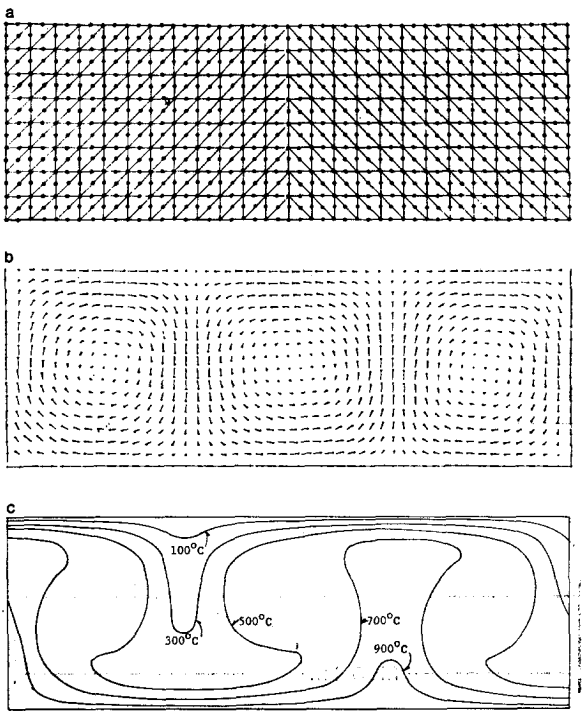

FIG. 6. Example 4, use of fine mesh to obtain numerical stability. (a) Mesh layout, (b) Three-cell velocity field, (c) Three-cell isotherms.

In this particular example the mesh was uniformly doubled in both the vertical and horizontal directions. A savings in computer time would result however, if the mesh were designed to specifically accommodate the three cell pattern, i.e., a slightly larger spacing between nodes in the center region of each cell, thus reducing the total number of algebraic equations.

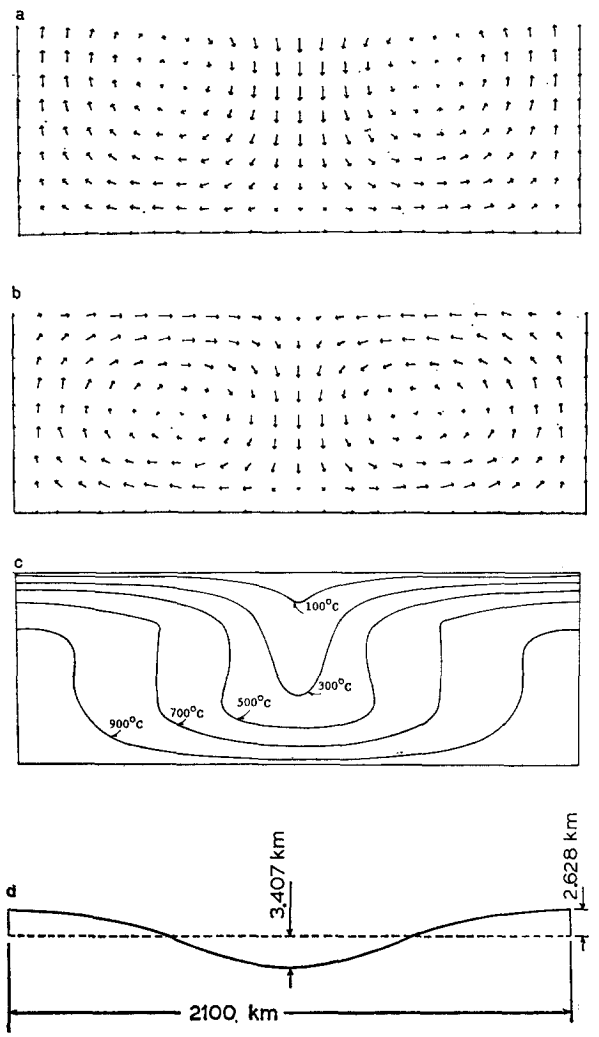

FIG. 7. Example 5, free surface flow. (a) Initial velocity (b) Steady-state free surface flow, (c) Isotherms, (d) Free surface profile.

Also of interest is the fact that a two cell configuration for this example could not be sustained.

Free Surface Flow—Example 5

The free surface techniques described earlier were used for the problems of Example 3. After the steady-state solution shown in Fig. 5(b) had been determined, the constraint on the upper boundary was removed. The temperature distribution of Fig. 5(c) then resulted in the "free-surface" velocity field shown in Fig. 7(a). It is clear from this figure that the free surface is not a streamline, a requirement necessary for steady-state conditions.

From this point on, the quasi-Lagrangian formulation was used to move the nodal point coordinates forward in time. The maximum displacement used during one increment was limited to 0.5 km. Figure 7(b) shows the final velocity field obtained after 10 increments of time. At this point nearly all the free surface velocities are tangent to the surface—that is, the surface has become a streamline indicating a near steady-state condition for the surface profile. The corresponding isotherms are shown in Fig. 7(c).

Because the mean density of the fluid was subtracted in this formulation, the gravity effects brought about by the surface topography were accounted for by a surface pressure proportional to the change in elevation from the mean. However, this is not necessary if the total density of the fluid is used in the formulation.

For this particular problem, the changes in surface profile are small compared to the dimensions of the problem. This profile is shown with an exaggerated vertical dimension in Fig. 7(c).

It should be noted that there are insignificant differences in the velocity and temperature fields obtained from the smooth boundary conditions and those obtained from the free boundary conditions. This reflects the fact that there was very little change in the problem geometry. For the study of flow in the near vicinity of ridges or trenches, for instance, free surface geometry could become very important. An example of the analysis of very large geometry changes due to creeping viscous flow is presented by Thompson and Haque [8].

5. Conclusion

The five examples presented in the previous section demonstrate the applicability of the finite-element method to the study of creeping convection. The ability to use either a quasi-Lagrangian or an Eulerian reference frame is particularly advantageous. Free surface boundary conditions are easily handled. The method should prove valuable for studies related to mantle convection and plate tectonics.

ACKNOWLEDGMENTS

This paper is based on research supported by the Earth Sciences Section, National Science Foundation, NSF Grant GA 41802. Acknowledgment is also due the Brazilian National Council of Research—CNP_q for providing a fellowship for Atuo Sato.

REFERENCES

1. D. J. ANDREWS, Numerical solution of sea floor spreading, *J. Geophys. Res.* **77** (1972), 6470–6481.
2. THEODORE D. FOSTER, The effects of initial conditions and lateral boundaries on convection, *J. Fluid Mech.* **37** (1969), 81–94.
3. L. R. HERRMANN, Elasticity equations for incompressible and nearly incompressible materials by a variational theorem, *AIAA J.* (1965), 1896–1900.
4. T. J. R. HUGHES AND H. ALLIK, Finite element for compressible and incompressible continua, *in* Proc. Symp. Applic. Finite Element Meth. Civil Engineering, Vanderbilt University, Nashville, 1969.
5. D. P. MCKENZIE, J. M. ROBERTS, AND N. O. WEISS, Convection in the Earth's mantle: towards a numerical simulation, *J. Fluid Mech.* **62** (1974), 465–538.
6. J. T. ODEN, Finite plane strain of incompressible elastic solids by the finite element method, *Aeron. Quart.* **XIX** (1968), 254–264.
7. ERIK G. THOMPSON, Average and complete incompressibility in the finite element method, *Int. J. Numer. Meth. Eng.* **9** (1975), 925–932.
8. ERIK G. THOMPSON AND M.I. HAQUE, A high order finite element for completely incompressible creeping flow, *Int. J. Numer. Meth. Eng.* **6** (1973), 315–321.
9. ERIK G. THOMPSON, LAWRENCE R. MACK, AND FONG-SHENG LIN, Finite element method for incompressible slow viscous flow with a free surface, *in* "Developments in Mechanics 5," Proc. 11th Midwestern Mechanics Conference, pp. 93–111. Ames, Iowa, 1969.
10. K. E. TORRANCE AND D. L. TURCOTTE, Thermal convection with large viscosity variations, *J. Fluid Mech.* **47** (1971), 113–125.
11. DONALD L. TURCOTTE AND E. R. OXBURGH, Mantle convection and the new global tectonics, *Ann. Rev. Fluid Mech.* **4** (1972), 33–68.
12. O. C. ZIENKIEWICZ, "The Finite Element Method in Engineering Science," McGraw–Hill, London, 1971.